An Eulerian-Based Formulation for Studying the Evolution of the Microstructure under Plastic Deformations

S. Ahmadi[1], B.L. Adams[1] and D.T. Fullwood[1]

Abstract: In this paper, a model is introduced to examine the evolution of the microstructure function under plastic deformations. This model is based upon a double continuity relationship that conserves both material particles in the mass space and orientations in the orientation space. An Eulerian description of the motion of material particles and orientations is considered, and continuity relations are derived for both spaces. To show how the proposed model works, two different case studies are provided. In the mass space, the continuity relation is used to examine the evolution of the microstructure function of a two-phase (isotropic) material; while, in the orientation space, this model is used to simulate the evolution of the microstructure of a randomly textured fcc material that has been cold rolled to a rolling reduction of 70%. In addition, in both case studies, our Eulerian continuity model is compared against the Lagrangian models that are widely used in the literature for texture predictions. Results show that by selecting an appropriate grid size for both workspaces the proposed Eulerian continuity model can accurately predict the evolution of the microstructure for large plastic deformations.

Keywords: Microstructure, Microstructure Function, Continuity Equation, Conservation Principles, CMC.

1   Introduction

Polycrystalline materials are aggregates of numerous crystallites or grains of various sizes and shapes. In order to study mechanical and metallurgical properties of polycrystalline materials one needs to know detailed information about the sizes, shapes and placement of these crystallites or grains. A grain in a polycrystalline material, by definition, is an aggregate of neighboring particles having similar crystallographic orientation with respect to the sample coordinate system. Study of the behavior of grains during deformation processes has been a pervasive subject of

---

[1] Brigham Young University, Provo, UT, U.S.A.

mechanical and materials sciences. Applying a plastic deformation causes particles of individual grains inside an examined polycrystalline material to move from their preliminary location to a new position in the space of material particles which is called *the real space* or *the mass space*. The deformation process, on the other hand, causes grains of the polycrystalline material to rotate around a specific rotation axis, to change their original orientation, and to take new configurations relative to the sample coordinate system. These changes are not random and involve rotations which are directly related to the crystallography of the deformation. As a consequence, the grains acquire a distinguishing pattern, or *texture*, which becomes stronger as deformation proceeds. These rotations take place in *the orientation space*, the space that includes all possible rotations of orientations. There are many ways to show the continuous motion (or rotation) of orientations, among which the *Euler angle space (EAS)* [Bunge (1993)] and the Rodrigues vector representations [Morawiec and Field (1996)] are more common in microstructure simulations. In this paper, the EAS is selected as the working space for orientation rotations.

From the discussion above, it can be concluded that for any material point in the material, there are two spaces that should be considered during the evolution process: the mass space and the orientation space. Conservation principles can be used to study the motion of material particles in the real space and lattice orientations in the orientation space.

In the real space, the motion of material particles is monitored by the mass-based continuity equation, which has been derived based upon the conservation of mass principle. The main application of this continuity equation is the solution to Navier-Stokes equations in fluid mechanics [Kreiss and Lorenz (2004)]. Navier-Stokes' equations commonly consist of five equations: three momentum equations, the continuity equation, and the constitutive equation. In the derivation of Navier-stokes equation, the continuity equation can be expressed in either a material (Lagrangian) or spatial (Eulerian) framework; and it can be used to monitor the motion of particles for a compressible or an incompressible fluid. The continuity equation has been applied mostly for linearly viscous fluids in the literature [Kreiss and Lorenz (2004); Irgens (2008); Lai, Rubin and Krempl (1993)]; and its application for solid materials is not common. In the current paper, we will introduce the mass-based continuity equation and will show how it can be employed to model changes in microstructure that occur with large deformations.

In the orientation space, we deal with rotations and lattice orientations. There have been many investigations on the evolution of grain orientations or the texture evolution of polycrystalline materials. The main tool exploited to quantify the crystallographic texture of material particles in the microstructure is the *orientation distribution function (ODF)* defined in the orientation space. The orientation dis-

tribution function, $f(g)$, by definition, is the volume density of material particles in the microstructure that associates with orientation g:

$$f(g)dg = \frac{dV}{V} \tag{1}$$

where dV/V denotes the volume fraction of the microstructure that is associated with local states lying within an invariant measure dg of orientation g. The orientation g in the Bunge-Euler space is specified by three Euler angles: $g = g(\varphi_1, \Phi, \varphi_2)$ [see Bunge (1993)].

Modeling texture evolution has been the subject of many studies for about three decades. Most of these models have been expressed in the Lagrangian framework [i.e. Kalidindi and Anand (1992); Kalidindi, Bronkhorst and Anand (1992); Kalidindi and Anand (1994)]. In these models the initial ODF is measured experimentally from the original microstructure, some plasticity-related models are exploited, and the final ODF is predicted by applying the plastic strain gradually. Lagrangian models have some benefits and limitations. The most serious limitation of using the Lagrangian system is that the shape and the size of the material volume element may change throughout the deformation process leading to a severely distorted mesh at the end of the process. Our preference here is to use an Eulerian framework in which a fixed control volume is considered and the rate of change of any material property, e.g. the mass density or the ODF, is studied in a permanent coordinate system.

The first approach to predict the evolution of the ODF using an Eulerian framework was proposed by Clement and Coulomb [Clement and Coulomb (1979); Clement (1982)]. Their model predicts the texture evolution considering a continuity relation that is valid in the EAS, and guarantees the conservation of orientation principle during the evolution. This continuity relation has been formulated from concepts commonly used in continuum mechanics to observe the rate of change of mass flowing in a continuous medium.

Based on Clement's formalism and the continuity equation in the orientation space, many studies have investigated the evolution of crystallographic texture for various deformation processes, such as uniaxial tension [Savoie, Zhou, Jonas and Macewen (1996)], plane-strain compression [Bunge, Esling, Dahlem and Klein (1986)], rolling [Wierzbanowski, Clement (1984); Wierzbanowski, Ahzi, Hihi and Berveilier (1986); Gilormini, Toth and Jonas (1990); Zhou, Toth and Neale (1992), Morawiec, Wierzbanowski, Jura and Baczmanski (1991)], simple shear or torsion [Baczynski and Jonas (1996); Beausir, Toth and Neal (2007); Arzaghi, Beausir and Toth (2009)], and deep drawing [Zhou, Jonas and Neale (1995); Choi, Cho, Oh, Chung and Barlat (2000)]. A power-law viscoplastic relation has been employed in

most of these models to generate the rotation rate field in the EAS. The rotation rate field and the orientation-based continuity equation have then been used to study the orientation stability of specific texture components of various (mostly fcc and bcc) materials. In this body of work, the orientation-based continuity equation has been used only to predict the ODF of stable texture components at the end of the process. In the EAS, if the velocity vector is defined as $w = w_i(g)$, an orientation $g*$ remains stable throughout the deformation if the following conditions are met: first, all of the components of the velocity vector go to zero, $w_i(g*) = 0$; and secondly, the slope of velocity components in the EAS stay negative during the process, or $\partial w_1/\partial \varphi_1 \leq 0$, $\partial w_2/\partial \Phi \leq 0$, $\partial w_3/\partial \varphi_2 \leq 0$ [see Clement (1982)]. In Section 5 and Appendix C, we have described our derivation of the orientation-based continuity equation in the space of Eulerian coordinates. It can be seen that both the velocity term and partial derivatives appear in the continuity equation (Eq. 11). It is discovered that when the velocity components become zero, the second term in the continuity equation vanishes and the numerical simulations for studying ideal orientations or stable texture components are simplified. Accordingly, the continuity equation can be used to study stable orientations with no difficulty.

However, if studying the evolution of a random texture or a random orientation is important, the second term in the continuity equation will not be zero, and it necessarily must be computed. A discrete framework can be established to approximate these partial derivatives. Although the continuity equation has been used in the literature to study the stability of ideal orientations, it has not been employed to statistically study the microstructure of materials. A discrete representation of mass- and orientation-based continuity equations in the basis of Eulerian coordinate system is introduced in this paper. This is a new hypothesis that has not been conceived in the past; and it can be exploited to study microstructure evolution of polycrystalline materials,

In the present paper, we will also show that instead of the ODF one can use another statistical function, called the microstructure function (MF), which represents the ODF at a specific material point. In this way one can consider a local ODF for any material point in the microstructure; and instead of texture evolution, the evolution of the MF can be studied locally. The MF, in addition to the 2-point correlation function, which is used in statistical continuum theory to study the local effects of one material particle on the properties of the neighboring particle, are introduced in Section 2. Then, the conservation of mass principle and the mass-based continuity equation is introduced in Section 3. To study the evolution of the MF only in the mass space, a model was established using the mass-based continuity equation. This model can be used to predict the evolution of the MF under large levels of plastic strain. The way this model works is described in detail in Section 4. Our

derivation of the orientation-based continuity equation in the EAS is discussed in Section 5. To validate the orientation-based continuity relation, rolling deformation of a randomly textured fcc material is modeled using our Eulerian model and a Lagrangian model. Details of establishing an Eulerian framework in the EAS and employing the continuity model for texture prediction of this random microstructure is presented in Section 6. More detailed formulation of continuity equations for the mass space and the EAS can be found in Appendices A and C, respectively. Appendix B provides the reasons of choosing a forward-backward finite difference method exploited in computations of the rate changes of the MF in the Eulerian model.

2 Microstructure representation

2.1 Microstructure function

The microstructure function (MF) is a statistical function used to express the volume fraction of a local state in the vicinity of a material point [Adams, Gao, and Kalidindi (2005); Fullwood, Niezgoda, Adams and Kalidindi (2009)]. Typical examples of local state can be phase, grain orientation, composition, and any other relevant local parameters. Lattice orientation is taken as the local state variable of interest in this paper consistent with the definition of the ODF. Formally, the microstructure function is defined as:

$$M(x,g)dg = \frac{dV_g}{V} \tag{2}$$

where V is the volume of the local neighborhood of material particle x, and dV_g is the volume of the local neighborhood within V that is associated with orientations that lie within an invariant measure dg of orientation g. The invariant measure in both Eqs. 1 and 2 can be expressed as $dg = \sin\Phi d\varphi_1 d\Phi d\varphi_2$ in the EAS. As one of the properties of the MF, integrating the MF in the entire volume of interest, one obtains the volume fraction of orientation g in the entire microstructure, which is the familiar ODF:

$$\frac{1}{V(\Omega)} \int_{\Omega} M(x,g)dx = f(g)|_{\Omega} \tag{3}$$

where Ω denotes the region of interest in the real space. This MF can be used in statistical continuum theory to express correlation functions.

2.2 1- and 2-point correlation functions

The simplest of the statistical functions used to quantify the microstructure are the 1-point distributions. The one point distribution function, which is also the familiar

ODF or the texture function (Eqs. 1 and 3), essentially reflects the probability density associated with realizing a specified orientation in the neighborhood of a point thrown randomly into the microstructure.

Another important statistical function is the 2-point correlation function, $f_2(g, g'|r)$, that denotes the probability density associated with finding specific local states g and g', respectively at the tail and the head of a vector r placed randomly into the internal structure of the material [Kroner (1967); Adams, Gao and Kalidindi (2005); Fullwood, Niezgoda, Adams and Kalidindi (2009)]:

$$f_2(g, g'|r) = \frac{1}{V(\Omega)} \int_{\Omega} M(x, g) M(x+r, g') dx \qquad (4)$$

Higher order correlation functions, also referred to as n-point spatial correlation functions have been also defined in the literature [Adams, Canova and Molinari (1989); Adams, Xiang and Kalidindi (2005)]. In this paper the 2-point correlation functions are used to study the local effects on the microstructure.

3   Conservation of mass

The principle of conservation of mass states that the total mass of any part of a body does not change with any motion. The mathematical form of this principle is different in material and spatial descriptions of motion. One benefit of using the Eulerian coordinate system for computations is that one can discretize the volume of interest using square-shaped, evenly-spaced grids, facilitating the use of fast Fourier transforms (FFTs) for economical calculations [Fullwood, Kalidindi, Niezgoda, Fast and Hampson (2008)]. Another benefit is that we can use the finite difference method (FDM) to approximate first-order partial derivatives that appear in the continuity equation.

The derivation of the mass-based continuity equation for the spatial description is shown in Appendix A. Using the definition of the material time derivative D/Dt, and taking a control volume in the Eulerian coordinates, the mass-based continuity equation is expressed as (Eq. 21 in Appendix A):

$$\frac{\partial \rho(x)}{\partial t} + div(\rho(x)v(x)) = 0 \qquad (5)$$

where $\rho(x)$ is the mass density and $v(x)$ is the velocity of the material particle x in the mass flow field. Using the divergence law the continuity equation becomes:

$$\frac{\partial \rho(x)}{\partial t} + \rho(x)\frac{dv_i(x)}{dx_i} + v_i(x)\frac{d\rho(x)}{dx_i} = 0 \qquad (6)$$

In fluid mechanics, the fluid is comprised of material particles that can be compressible or incompressible. However, in solid materials, to a very good approximation the polycrystalline material can be considered to be an incompressible material, and hence the term $v_{i,i} = dv_i/dx_i$ approaches zero; thus we have:

$$\frac{\partial \rho(x)}{\partial t} = -v_i(x)\frac{d\rho(x)}{dx_i} \tag{7}$$

This equation is the final form of the mass-based continuity equation for an incompressible material.

4   Application to a two-phase material

The continuity equation formulated in the previous section can be used to predict the evolution of the MF for a two-isotropic-phase (TIP) material. We assume that the microstructure is composed of two regions each representing a phase (Fig. 1a: white and black area indicate phase 1 and 2, respectively). To build a model based upon the continuity equation for the TIP material, the following assumptions are made: (1) the material under deformation acts like an incompressible media; (2) the phases do not change from one to the other during the deformation process; (3) the phases have isotropic properties; and (4) the motion of phase particles is a continuous process. In addition, the continuity equation is readily extended from Eq. 7 to apply to the MF:

$$\frac{\partial M(x,g*)}{\partial t} = -v_i(x)\frac{dM(x,g*)}{dx_i} \tag{8}$$

where specifying $g*$ indicates that we have derived the equation for a particular orientation (or phase here). If phase change does not occur during deformation, the continuity equation can be expressed for each phase individually. We will hereafter focus on the continuity equation for the second phase expressed in Cartesian coordinates.

The TIP model is constructed for a plane-strain compression test (similar to rolling). A plane-strain compression test has two planes of symmetry and four regions that material particles are symmetrically moving in each of these regions. In this study, the upper right corner of a plane-strain test is sampled. Accordingly, since plane-strain condition is applied, plastic strain in the 2-direction is assumed to be zero ($\varepsilon_2 = 0$) and based upon the incompressibility we will have $\varepsilon_1 = -\varepsilon_3$. Assuming that the macroscopic motion conditions also apply locally (following the familiar Taylor hypothesis), the equations of motion throughout the material are then simplified to $x_1 = X_1 \exp(\dot{\varepsilon}t)$, $x_2 = X_2$, and $x_3 = X_3 \exp(-\dot{\varepsilon}t)$. Here $\dot{\varepsilon}$ is the applied strain

rate, x represents the position of a material particle with respect to a pre-defined Eulerian coordinate system at time t, and X shows the position of that particular material particle at the reference configuration ($t = 0$). Based upon the definition of velocity $v_i = dx_i/dt$, the velocity components can then be obtained: $v_1 = \dot{\varepsilon}x_1$, $v_2 = 0$, and $v_3 = -\dot{\varepsilon}x_3$. Equations of motion also provide the boundary conditions required in the simulation. Three boundary conditions are required for modeling the upper-right region of a plane-strain compression test: (1) Material particles are not moving in the 2-direction during the process (i.e. $x_2 = X_2$ or $v_2 = 0$). (2) At the lower boundary, material particles are not allowed to move vertically. For this case since we have $X_3 = 0$, using the equation of motion $x_3 = X_3 \exp(-\dot{\varepsilon}t)$, we get $x_3 = 0$ and consequently $v_3|_{X_3=0} = 0$. Note that material particles can freely move in the 1- direction at this boundary. (3) At the left boundary, based upon the equations of motion, we will have $x_1 = 0$ and $v_1|_{X_1=0} = 0$, while material particles can move in the 3- direction. This can be seen in Fig. 1b.

Fig. 1b shows a section of the velocity field determined for the TIP model. To obtain this field, the real space is discretized into small bins. The velocity vector is calculated for each Eulerian point for a strain rate of $\dot{\varepsilon} = 0.001\,s^{-1}$. Once the velocity field is defined we can apply an iteration scheme to get the evolution of the microstructure. If the plastic deformation is applied in small steps of time we can rewrite the continuity equation as:

$$\frac{\Delta M(x)|_2}{\Delta t} = -v_1(x)\frac{dM(x)|_2}{dx_1} - v_3(x)\frac{dM(x)|_2}{dx_3} \tag{9}$$

where the notation $|2$ specifies that we are modeling the evolution of the MF for the second phase.

In the above equation the only unknown terms are the partial derivatives. To compute these derivatives a finite difference method (FDM) can be used. It was found that among all the finite difference schemes, forward and backward differences were the best choices. Distinguishing between the usage of forward or backward methods depends upon the sign of the velocity component. If velocity is positive, the backward difference is best; and if it is negative, the forward difference method should be used. An example that can clarify reasons of choosing this finite difference scheme is provided in Appendix B. When all terms are calculated, the change of the microstructure function at one time step can be calculated from Eq. (9), and simply the microstructure function at the end of the iteration is calculated by $M_f = M_i + \Delta M$ where ΔM is calculated from Eq. 9, assuming that $\Delta t = 1$. For simplicity, it was assumed that the deformation is a steady process with a uniform velocity field that does not change as deformation proceeds. Then, to obtain an exact amount of strain this process is iterated until the total strain is reached. For

instance, if we assume that the strain rate is $\dot{\varepsilon} = 0.001\,s^{-1}$, to apply a total plastic strain of 10%, the number of iterations will be 100. The final microstructure function is eventually captured from the last iteration.

Fig. 1 demonstrates the evolution of microstructure function for the TIP model. Micrograph (a) shows an area ($15 \times 15\ \mu\text{m}^2$) taken from the original microstructure. The microstructure is discretized into equally-spaced bins with 0.3 μm grid size. The MF at every bin is set to 0 if phase 1, and 1 if phase 2 fills the bin. If the bin contains a fraction of phase 1 and 2, its MF takes a value based on the fraction of phase 2. MF evolution is progressed using Eq. 9 and the iteration scheme that was described. The evolution of microstructure for different amounts of total strain is shown in subplots (c-e). It can be seen that as the deformation proceeds, the MF becomes more diffuse near interfaces.

To validate our model for predicting MF evolution, another model can be established that will provide the final microstructure without applying any iteration technique. For this model, which has a Lagrangian basis, about 100 points were thrown randomly into every bin in the initial microstructure. These points are labeled as phase 1 or 2 based on their original location. If we know the final amount of strain that should be applied, the number of total iterations is also determined, then the final location of points can be determined using the equations of motion. For example, if we take a point at position (2,0,2) and if it is desired to apply 10% strain at the rate of $\dot{\varepsilon} = 0.001\,s^{-1}$, 100 iterations are required. Based upon the equations of motion, this point at the end of process is located at (2.21 0 1.81) because e.g. $x_1 = 2\exp(0.001 \times 100) = 2.21$. These points were forced to move directly using the equations of motion. The final MF then was calculated for each Eulerian bin by finding the fraction of the number of points belonging to phase 2 relative to the number of all points occupying that bin. A comparison of final microstructure predicted by the continuity relations and the second (direct) model, is illustrated in Fig. 2 (a and b).

The 2-point correlation function between phase 1 and 2, $f_2(1,2|r)$ was also computed using FFTs; for more information regarding the implementation of FFTs in manipulating the 2-point functions the reader is referred to the work of Fullwood et al. [Fullwood, Kalidindi, Niezgoda, Fast and Hampson (2008)]. The f_2 plots for both models are shown in Fig. 2 (c and d). In the microstructure predicted by the continuity relations, some spreading of the second phase (similar to a diffusion phenomenon) can be seen on the boundaries. The smearing happens during the iteration scheme. It initiates from the use of finite difference methods. There is not an explicit way to calculate partial derivatives in Eq. 9. Using finite difference method gives an error of the order of the bin size at every step of deformation. This error accumulates with the number of calculation steps, and results in a thicker smeared
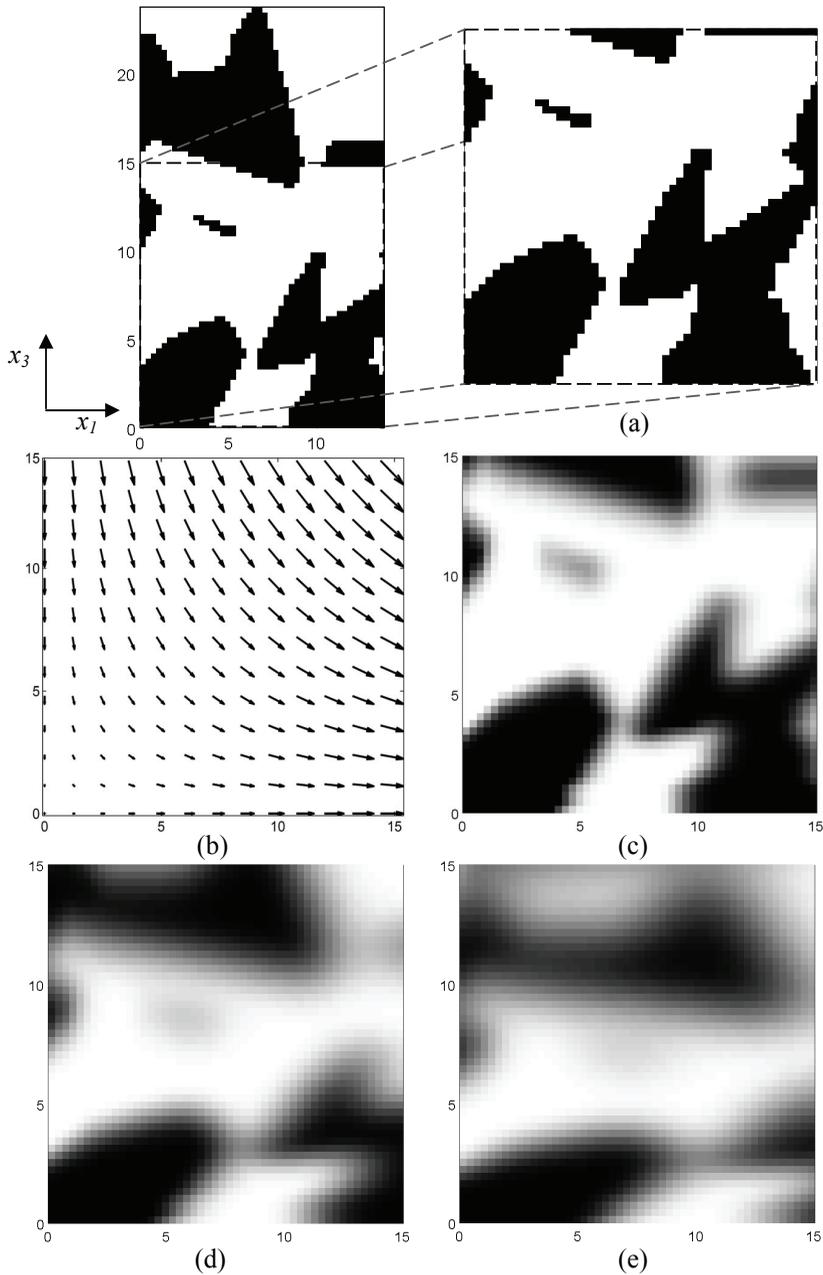
Figure 1: MF evolution under plane-strain conditions for the two phase model (white: phase 1; black: phase 2). (a) initial MF; (b) velocity field for the plane-strain condition; (c, d, and e) MF evolution after 10%, 30%, and 50% total strain.

boundary layer as a function of the number of iterations. The extent of these errors depends upon the number of iterations and the bin size. This smearing effect is more obvious in Fig. 1 (c-e) where different amounts of strain are applied.
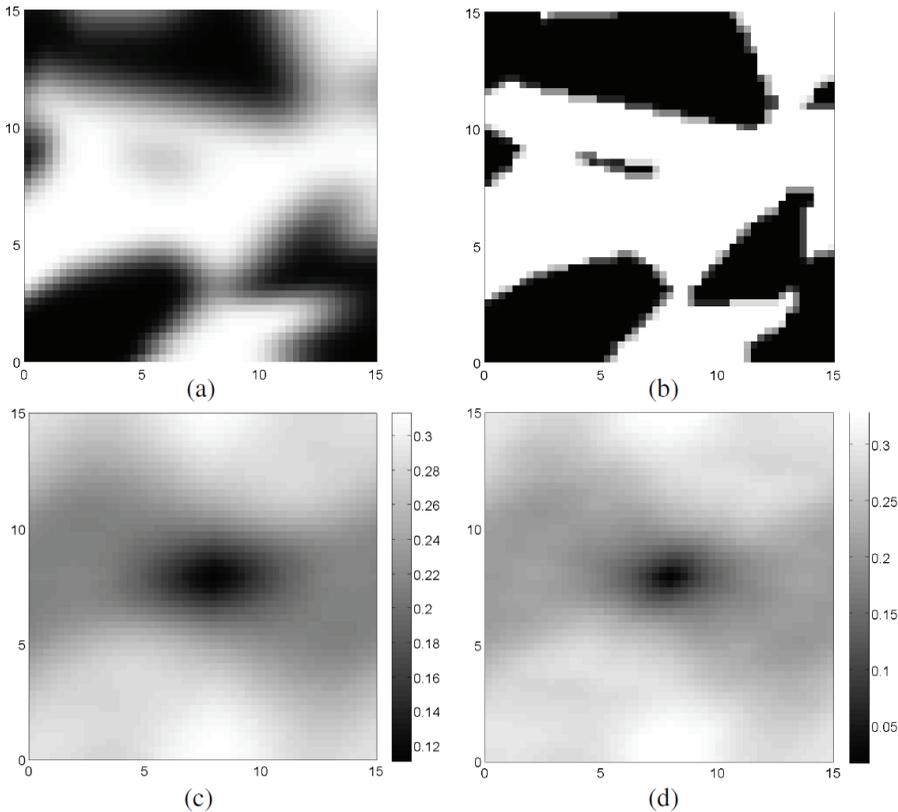

Figure 2: MF evolution for 30% total plastic strain predicted by (a) continuity relations; (b) the direct (Taylor) model; (c and d) 2-point correlation function plots for Eulerian-based continuity model and the direct model, respectively.

Fig. 3 shows the error plot representing the absolute error between the f_2 obtained from the two models. It can be observed that the maximum absolute error for 30% total strain is about 9.4 %. This maximum error occurs for small vectors r, with ends that land on phase 1 and 2, which samples the region between the two phases, or the boundaries. If we neglect the smearing effect on the boundaries, the mean absolute errors is about 0.8% which is reasonably acceptable. It is concluded that if the effect of boundary spreading somehow can be resolved, the continuity model can provide precise predictions of MF evolution under large deformations. Control

of boundary layer thickness can be addressed by either choosing a smaller grid size or applying fewer iterations (with larger strain applied in each step). On the other hand, there is a limit on the maximum amount of strain that can be applied in one time step. It can be shown that the maximum strain needs to be consistent with the limit that $v_i \Delta t \leq d$ where d is the bin size. The velocity field in this study is steady; hence it can be shown that as the time step increases, the binning size has to increase as well. Therefore, only one parameter remains that can control the process, which is the bin size.
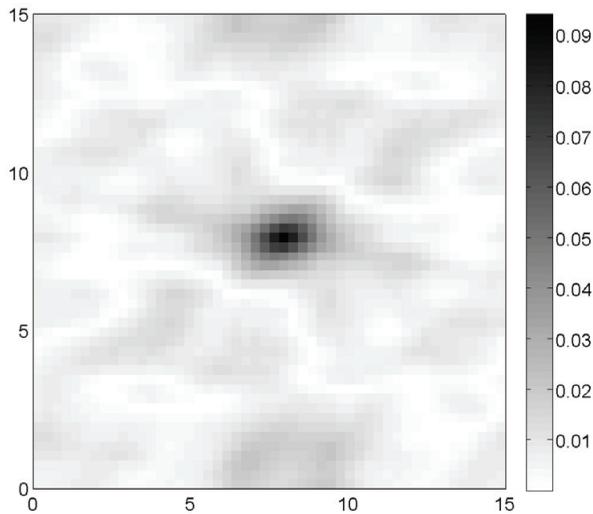

Figure 3: Error plot showing the absolute error of the 2-point correlation functions for the two models.

The effect of bin size on the accuracy of our model was studied in Fig. 4. A variety of grid sizes were chosen from 0.3 to 0.0375 microns. The original microstructure was deformed to a total strain of 30% in 300 iterations. One can see that choosing smaller grids will help to enhance the resolution and reduce the effect of boundary spreading. Tab. 1 also shows the binning effect on the resolution and the time of process. Calculations were conducted on a regular PC. Taking smaller grid size increases processing time dramatically, but results in less error. The times shown in here are for a 2-D model; it is anticipated that a 3D model would demonstrate a significant amplification of the trend in calculation times.

An optimum case of selection of binning size should be taken to achieve good resolution with a reasonable error and an acceptable processing time. For the present study with a selection of grid size of about 0.075 microns results in an appropriate
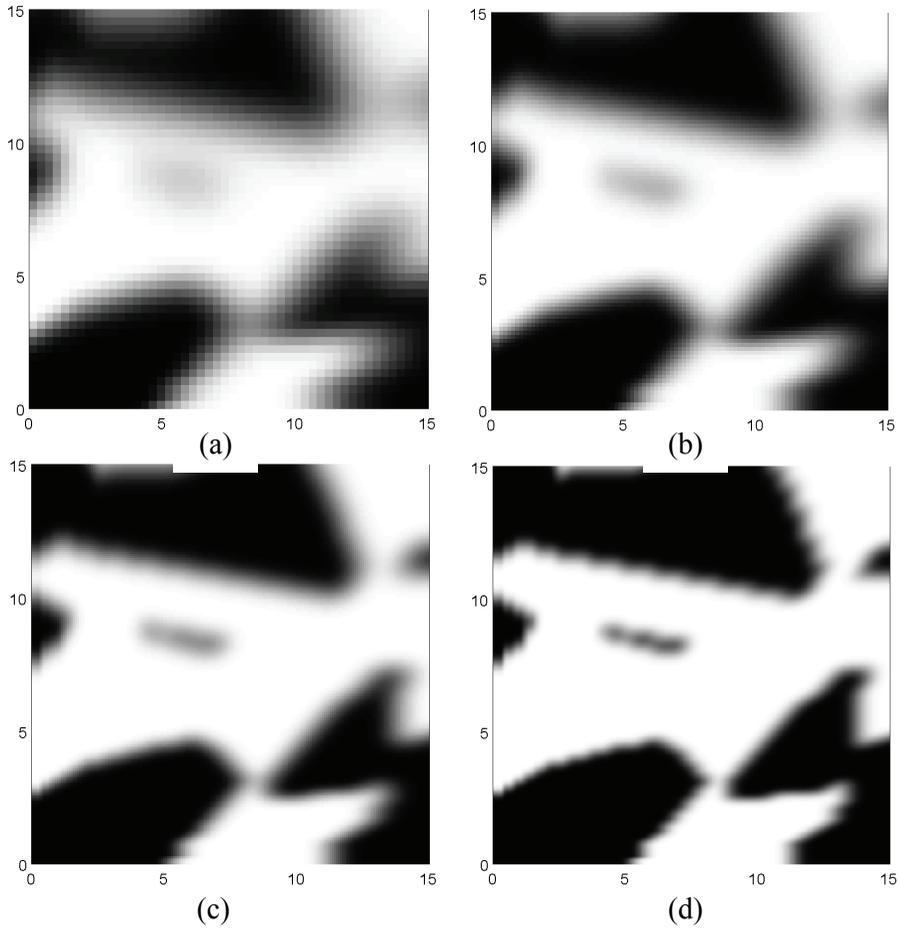
Figure 4: MF after 30% total plastic strain with different grid sizes: (a) 0.3; (b) 0.15; (c) 0.075; (d) 0.0375 microns.

Table 1: Effect of binning size on the accuracy of the proposed model.

Mesh size (μm)	0.3	0.15	0.075	0.0375
Maximum Absolute Error (%)	9.39	7.49	5.64	4.01
Mean Absolute Error (%)	0.79	0.48	0.27	0.13
Calculation Time (sec)	3	8	19	52

simulation time with $\sim 5\%$ error.

The absolute error between the 2-point correlation functions computed for both models is presented in Fig. 5. Evidently, smaller grid size minimizes the spreading effect, achieving a maximum absolute error of $\sim$5.6% by comparison to Fig. 3.
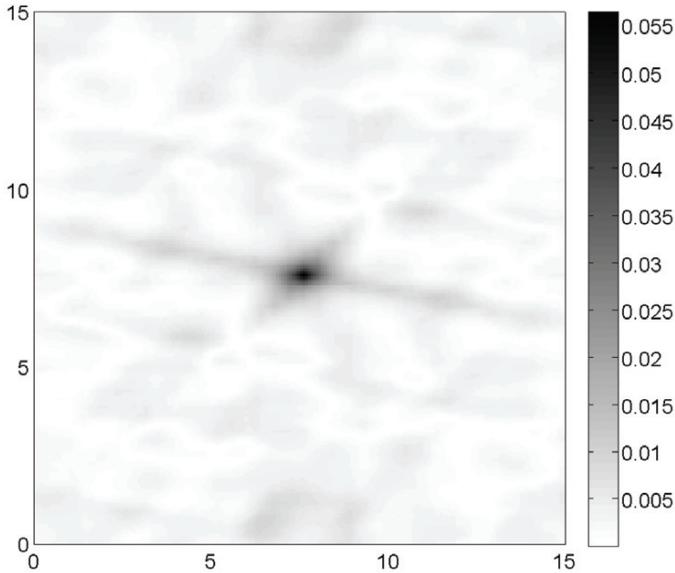

Figure 5: Error plot representing the absolute error of the 2-point correlation functions. The continuity model with 0.075 micron grid size is compared against the direct model.

5 Conservation of Orientation

Similar to the conservation of mass principle in the real space, a conservation of orientation is also suited for the orientation space. The continuity equation for orientations was first proposed by Clement and Coulomb [Clement and Coulomb (1979); Clement (1982)]:

$$\frac{\partial f}{\partial t} + div(fw) = 0 \tag{10}$$

where f is the ODF and w is the velocity vector in the orientation space. This equation is similar to the continuity equation in the real space (Eq. 2), and it guarantees the principle of conservation of orientations, meaning that crystallite orientation

may be altered, but neither created nor destroyed during plastic deformation. An Eulerian representation of the orientation-based continuity equation is presented in Appendix C assuming that the working space is the EAS. This derivation is proposed based on presuming the EAS to be a Riemannian Manifold. (In fact, the EAS can be expressed in either a Euclidean space or a Riemannian Manifold. A Riemannian manifold is a differential manifold on which a smooth field of symmetric and positive definite metric tensor is specified [Hicks (1965); Morawiec (2004)].) The divergence in the continuity equation can be formulated using the covariant derivative and Christoffel symbols. The final form of the continuity equation can be expressed for the EAS as (Eq. 30 in Appendix C):

$$\frac{\partial f(g)}{\partial t} = -f(g)\frac{\partial w_i(g)}{\partial g_i} - w_i(g)\frac{\partial f(g)}{\partial g_i} - f(g)\cot\Phi\, w_2(g) \tag{11}$$

The first term on the RHS represents the rate of change of the velocity vector in the EAS. Although we have an incompressible material in the real space and this term in the formulation of mass-based continuity equation was zero, the flow of orientations in the EAS is compressible and we should treat rotations of orientations as a compressible fluid process. Similar to the continuity equation in the mass space, finite difference methods can be used to compute the partial derivatives in Eq. 11. To find the velocity vector w and the rotation rate field in the EAS, various plasticity models can be used. The binning process is similar to the discertization scheme applied to the mass space. The EAS is discretized into a small size Eulerian grid. The center point of each bin is then taken as the Eulerian point and the velocity vector is calculated for all bins in the Euler angle domain.

The orientation-base continuity equation (Eq. 11) has been used to find the evolution of the ODF. Following a process similar to our formulation in Section 3, Eq. 11 can be extended to describe the evolution of the MF for a specific material particle x:

$$\frac{\partial M(g)}{\partial t}\Big|_x = -M(g)|_x\frac{\partial w_i(g)|_x}{\partial g_i} - w_i(g)|_x\frac{\partial M(g)|_x}{\partial g_i} - M(g)|_x\cot\Phi\, w_2(g)|_x \tag{12}$$

This equation can be used to find the evolution of the MF at every material particle x. The double continuity relationship can be obtained by linking Eqs. 8 and 12 together. For a polycrystalline material, the motion of its material particles can be studied using Eq. 8, and at the same time, its evolution of grain orientations can be examined using Eq. 12. As long as the velocity fields and partial derivatives in Eqs. 8 and 12 are calculated in both working spaces, we will be able to make a prediction of the microstructure evolution for polycrystalline materials under any

form of plastic deformation. A simple example of using Eq. 12 for texture predictions, without taking into account the location of material particles, is presented in the next section.

6 Application to a randomly textured material

The Eulerian-based formulation of the continuity equation in the EAS was presented in the previous section. In this section, an example of obtaining the lattice rotation field (velocity field in the orientation space) and rotation of orientations under this field is explained. To find the velocity terms presented in Eq. 12 a crystal plasticity model should be used to find the lattice spin tensor. The lattice spin tensor is a rotation tensor that causes the rotation of crystallographic orientations under plastic deformation. A Taylor-like rate-dependent viscoplastic model is used here to obtain the lattice rotations. Based upon the Taylor assumption, the local strain applied into every grain in the microstructure is proportional to the macroscopic plastic strain applied into the entire microstructure [Taylor (1928)]; in addition a rate-sensitive viscoplastic model is linked to the conventional Taylor model to resolve the ambiguity of the Taylor model in finding five optimum activated slip systems [Asaro and Needleman (1985)]. The viscoplastic relation that we use is identical to that defined by Hutchinson [Hutchinson (1976)], where for a resolved shear stress, $\tau^{(s)}$, acting on the sth slip system, the slip shear rate, $\dot{\gamma}^{(s)}$, is connected by the equation:

$$\dot{\gamma}^{(s)} = \dot{\gamma}_0 \left(\tau^{(s)} / \tau *^{(s)} \right)^{1/m} sgn \left(\tau^{(s)} \right) \tag{13}$$

where m is the rate sensitivity parameter, $\tau *^{(s)}$ is called either the critical resolved shear stress or the slip resistance, and $\dot{\gamma}_0$ is an arbitrary reference slip rate. The reference shear stress can be obtained from ordinary tension or compression testing. To use the viscoplastic relation, it is necessary to calibrate the model with experiments [Fromm, Adams, Ahmadi and Knezevic (2009); Knezevic, Kalidindi and Fullwood (2008)]. We use the Taylor-like viscoplastic model to simulate the evolution of orientations for a fcc material under fully plastic deformation with slip systems of {111}<110>. The parameters appearing in Eq. 13 are taken as: $\dot{\gamma}_0 = 0.001 \sec^{-1}$, $m = 0.012$, and $\tau* = 35 MPa$. For simplicity, it is further assumed (1) that the critical resolved shear stress is identical for all slip systems; and (2) that the material is deformed under a rigid-perfectly-plastic condition without taking into account any slip hardening effects.

Simplified rolling process (e.g. taking a plane-strain compression condition) is modeled here to find the evolution of orientations in a randomly textured microstruc-

ture. In this case the velocity gradient tensor is defined as:

$$L^{app} = L_0 \begin{bmatrix} 1 & 0 & 0 \\ 0 & 0 & 0 \\ 0 & 0 & -1 \end{bmatrix} \tag{14}$$

where L_0 for the case of rolling is called the rolling deformation (the true stress in the rolling direction), and is taken to be $0.001\,s^{-1}$ in our calculations. Having defined the applied velocity gradient, it is assumed that the local velocity gradient is identical to the applied one (Taylor assumption), and the crystal orientation changes, i.e. the lattice spins, can be obtained by:

$$W^L = L^{app} - \sum_{(s)} M_{ij}^{(s)} \dot{\gamma}^{(s)} \tag{15}$$

where $M^{(s)} = b^{(s)} \otimes n^{(s)}$ is the Schmid tensor for the slip system s; while $b^{(s)}$ and $n^{(s)}$ are the unit slip direction and unit slip plane normal for the slip system s in the deformed configuration, respectively. Furthermore, the rotation velocity terms for every orientation in the EAS can be calculated by:

$$\begin{aligned} w_1 &= -\cot\Phi\sin\varphi_1 W_{32}^L + \cot\Phi\cos\varphi_1 W_{13}^L + W_{21}^L \\ w_2 &= \cos\varphi_1 W_{32}^L + \sin\varphi_1 W_{13}^L \\ w_3 &= \csc\Phi\sin\varphi_1 W_{32}^L - \csc\Phi\cos\varphi_1 W_{13}^L \end{aligned} \tag{16}$$

These velocity terms then can be used in two different ways to study the evolution of orientations: (1) A Lagrangian model with an iteration scheme can be constructed such that orientations at the end of each iteration are updated simply by summing up the amount of rotation caused by the lattice spins. In this way if we take the original orientation as g_i then the final orientation at the end of current iteration is obtained by $g_f = g_i + w.\Delta t$. (2) We can use the Eulerian formulation that was expressed in Section 5, along with the iteration scheme that was introduced for the mass-based continuity equation. In this case, to obtain the velocity field the conventional 3-fold redundant cubic fundamental zone space, FZ_{3C}, with parameters lying in the ranges of $0^o \leq \varphi_1, \Phi, \varphi_2 \leq 90^o$, was discretized into small cubic bins. Lattice rotations were calculated for centers of bins. A schematic representation of the rotation rate field calculated for the rolling process is shown in Fig. 6. This plot shows a 2D section of the 3-dimentional FZ_{3C} sliced at $\varphi_2 = 45^o$. After obtaining the velocity field, every orientation of the microstructure is placed into this field and the movement of the orientation is monitored by an iteration scheme (similar to the mass-based scheme).
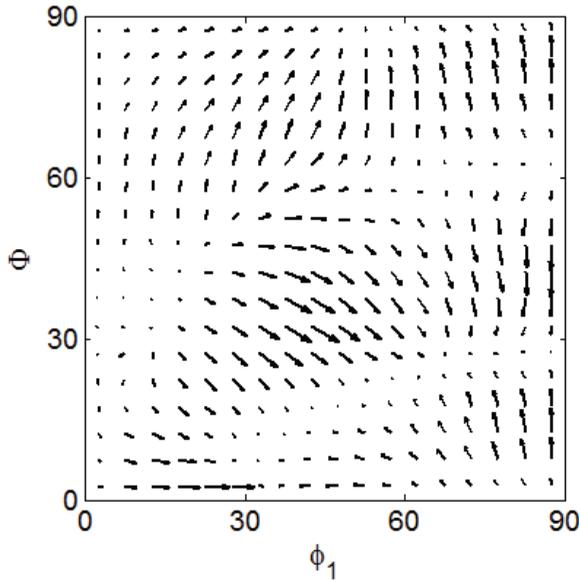
Figure 6: A 2D section plot of the conventional cubic FZ$_{3C}$ indicating the lattice rotation rate field of orientations in the $\varphi_2 = 45^o$ section.

To validate our proposed Eulerian model, a comparison against a Lagrangian model was performed. The comparison model selected is that used in most of FEM analyses [e.g. Kalidindi and Anand (1992); Kalidindi, Bronkhorst and Anand (1992); Kalidindi and Anand (1994)]. Evolution of the texture of a randomly textured microstructure with 1000 random orientations is studied with both models. These orientations are randomly taken from FZ$_{3C}$. The chosen microstructure is assumed to be rolled into the final reduction of 70% (rolling deformation of ~120%). Using the Lagrangian model, as it was explained, is straight forward. To employ the Eulerian model these steps are followed: (1) One orientation is studied at a time. The selected orientation is located in the conventional FZ$_{3C}$ and a cube with the size of 20×20×20 degrees is taken around the chosen orientation. The MF for this cube is set at 1 for the bin that contains the orientation and 0 everywhere else; (2) In addition to the velocity field, partial derivatives and all the terms presented in Eq. 12 are determined for the surrounding cube; (3) A finite difference scheme similar to the one introduced for the mass space is also employed here to find the evolution of the microstructure function; (4) To have an efficient model, the deformation process is subdivided into small increments in which 5% strain is applied in 500 time steps. At every time step, 0.1% true strain is applied; then, the rate change

of the MF is calculated and added up to the current value of the MF. This iterative process continues until it reaches the limit that is 5%. This gives one increment of the deformation that is equivalent to true strain of 5%. Because we use FDM in the iterative scheme, similar to the mass problem, smearing of the MF will occur; therefore, a cleaning process was designed here such that the bin having the maximum value of MF is taken as the final rotated orientation after 5% strain. (5) To apply further amounts of rolling deformation a new cube is taken around the updated orientation and previous steps (step 1-4) are repeated until the desired amount of deformation is reached. The final strain for applying 70% rolling reduction is ~120%; this amount of deformation is applied in 24 deformation increments. During this iterative process it must be anticipated that some of the orientations fall out of FZ_{3C}, for such cases the related crystal- and sample-symmetry operators are used to map the orientation back into FZ_{3C} after which the process continues on.

To statistically analyze results from Lagrangian- and Eulerian-based models (200) and (111) pole figures were constructed. A Gaussian distribution with a half-scatter width of 5°, and an orthorhombic sample symmetry was used in calculations of pole plots. All pole figures presented in this paper are equal area projections of the specified crystallographic poles. Fig. 7 shows the pole figures calculated for the randomly textured microstructure. Weak intensities in the pole plots admit that the microstructure is randomly textured.
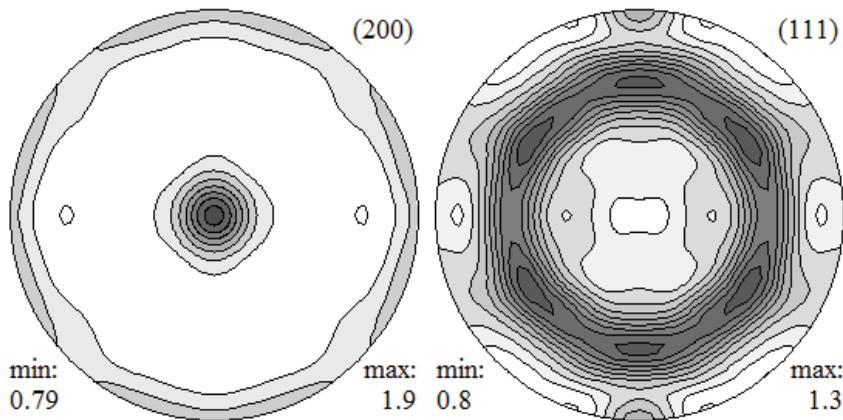

Figure 7: (200) and (111) pole plots calculated for the randomly textured microstructure.

The Lagrangian and Eulerian models were later used to predict the evolution of the texture of this microstructure. The pole figures predicted by the Lagrangian model

are illustrated in Fig. 8 (subplot a). To study the effect of binning size, the Eulerian continuity model with three different grid sizes was used. Fig. 8 (subplots b-d) is showing the binning effects for bin sizes of 1, 0.5, and 0.25 degrees (subplots b-d respectively).

From Fig. 8, it obviously can be seen that the Eulerian-based model can quantitatively give reasonable predictions of texture evolution (it can predict the locations of the high intensity peaks); however, because the pole plots predicted by larger mesh sizes show lower intensities compared to the ones predicted by the Lagrangian model, we suspect that the application of the Eulerian continuity model with too large mesh sizes may not adequately predict the quantitative details of texture evolution. Conversely, by decreasing the mesh size and taking smaller bins in FZ_{3C}, the resolution of the continuity model is increased.

In addition to the resolution effect, the computation time is also an important consideration. It can be proven that the algorithms of the Eulerian continuity model are more time-efficient. The total time spent for employing the Lagrangian model to simulate the 70% rolled macrostructure is ~7.5 hours on a standard PC. This time is mostly spent to find a solution for the nonlinear power-law equation (Eq. 13) using a Newton-Raphson scheme (e.g. [Fromm, Adams, Ahmadi and Knezevic (2009)]) and to calculate the lattice spins from Eq. 15. At each iteration, 0.1% strain is applied; therefore, there are 1000 orientations and 1.2/0.001=1200 iterations, which means that this nonlinear equation must be solved 1,200,000 times for this particular microstructure (If another microstructure is modeled all these calculations must be retaken). However, in using the Eulerian continuity model to build the rotation rate field, FZ_{3C} is discretized into 2 degree bins and the nonlinear equation is generally calculated $45 \times 45 \times 45 = 91,125$. If taking a smaller mesh size is desired, due to the fact that the rotation rate field is a continuous field and velocity terms are gradually changing from one bin to the other, we can take the midpoint of two adjacent grid points as the new point and the average velocities of the adjacent points can be assigned as its velocity. Total calculation time to construct the velocity field with 2 degree mesh size is ~36 minutes. This calculation is carried out only once and the velocity field is valid for simulating cold rolling of all types of fcc materials. In addition to this calculation time we should also include the time that is needed to update the MF by the iteration scheme, as explained earlier. Table 2, shows this calculation time and the amount of error that appeared from using the Eulerian continuity model compared to the Lagrangian model.

From Fig.8 and Tab. 2, it can be concluded that a mesh size of 0.5 degrees is optimal since the average absolute error is less than 1 degree and the overall time (including the time required to compute the rotation rate field) is reasonable: ~82 minutes. This computational time is a factor of ~5.5 less than the time spent in
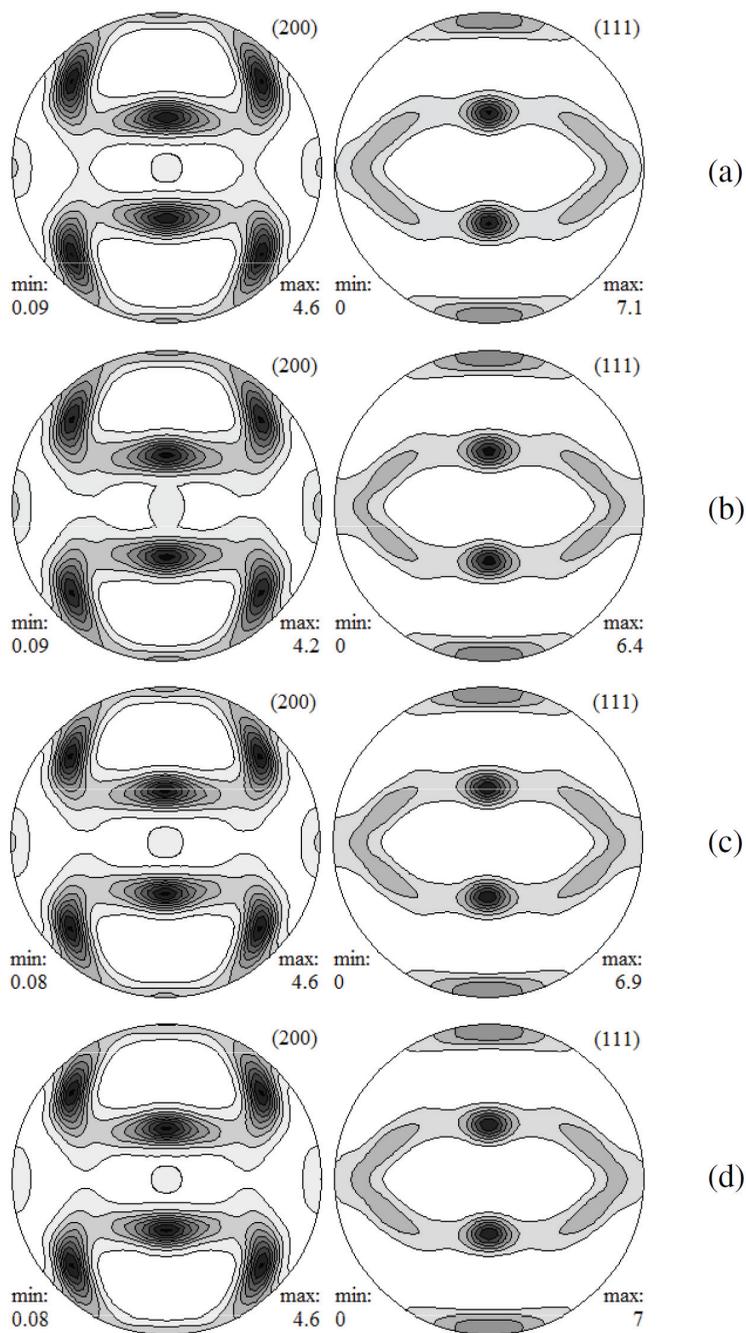
Figure 8: (200) and (111) pole plots predicted by: (a) Lagrangian model; Eulerian model with binning sizes of (b) 1 degree; (c) 0.5 degrees, and (d) 0.25 degrees.

Table 2: Effects of binning size on the accuracy and calculation time of continuity

Mesh size (degree)	1	0.5	0.25
Maximum Absolute Error (degree)	11.31	6.43	4.79
Mean Absolute Error (degree)	1.78	0.97	0.83
Calculation Time (min)	8	46	115

calculations by the Lagrangian model.

7   Conclusions

A new Eulerian model for predicting the evolution of microstructure under plastic deformation was presented. This model was established based upon the conservation principles in two spaces, the mass space, and the orientation space. Assuming the EAS as a Riemannian manifold, a new derivation of the orientation-based continuity equation was introduced. To examine the proposed continuity model two case studies were provided: (1) A limited 2-D example of the application of the model was presented. This example was offered to validate the mass-based continuity equation (Eq. 7). A two-isotropic-phase structure, without phase transformation, was studied under large plastic deformations. The framework of the model was validated against a direct calculation of particle motions. Results show that the accuracy is enhanced by choosing a mesh of small size. (2) Rolling deformation of a randomly textured aggregate including 1000 random orientations was studied using the Lagrangian- and Eulerian- continuity models. In this example, the aim was to only examine the orientation-based continuity equation. Predicted pole figures and results obtained from the comparison of Lagrangian and Eulerian models confirm that, as we were expecting from the two-phase example, the binning size has also an important effect on the accuracy of the continuity model in the orientation space. As the size of the bins decreases, the accuracy of the model and the overall processing time are increased. Results show that an optimum compromise is achieved when we choose a 0.075 micron mesh for the mass space and a 0.5 degree mesh in the orientation space. The two cases that are studied in this paper are examining the evolution of the MF in the mass and orientation spaces separately; however, one can realize that by coupling the two mass- and orientation-based continuity equations (Eqs. 7 and 12) the evolution of a polycrystalline material under any type of deformation process can be studied by using the Eulerian approach provided in this paper. This approach seems to be faster (and sufficiently accurate) compared to the Lagrangian approach that is used in FEM models. Another benefit of using the Eulerian approach is that, as explained, FFTs can be used in computing

the 2-point statistics that nowadays are commonly used to statistically analyze the microstructure of polycrystalline materials.

References

Adams, B.L., Canova, G.R., Molinari, A. (1989): A statistical formulation of viscoplastic behavior in heterogeneous polycrystals, *Texture and Microstructures*, 11, pp. 57-71.

Adams, B.L., Gao, X., Kalidindi, S.R. (2005): Finite approximations to the second-order properties closure in single phase polycrystals, *Acta Materialia*, 53, 13, pp. 3563-3577.

Arzaghi, M., Beausir, B., Toth, L. (2009): Contribution of non-octahedral slip to texture evolution of fcc polycrystals in simple shear, *Acta Materialia*, 57, pp. 2440-2453.

Asaro, R.J., Needleman, A. (1985): Overview no. 42 Texture development and strain hardening in rate dependent polycrystals, *Acta Metallurgica*, 33, pp. 923-953.

Baczynski J., Jonas J.J. (1996): Texture development during the torsion testing of a-iron and two if steels, *Acta Materialia*, 44, 11, pp. 4273-4288.

Beausir, B., Toth, L., Neale, K.W. (2007): Ideal orientations and persistence characteristics of hexagonal close packed crystals in simple shear, *Acta Materialia*, 55, pp. 2695–2705.

Bunge, H. J. (1993): Texture analysis in materials science, Mathematical Methods, Cuvillier Verlag.

Bunge, H.J., Esling, Dahlem, Klein (1986): The Development of Deformation Textures Described by an Orientation Flow Field, *Textures and Microstructures*, 6, pp. 181-200

Choi, S.H., Cho, H.H., Oh, K.H. Chung, K., Barlat, F. (2000): Texture evolution of FCC sheet metals during deep drawing process, *Int. J. Mech. Sci.*, 42, pp. 1571-1592.

Clement, A. (1982): Prediction of Deformation Texture Using a Physical Principle of Conservation, *Materials Science and Engineering*, 55, 1982, pp. 203-210.

Clement, A., Coulomb, P. (1979): Eulerian simulation of deformation textures, *Scripta Metallurgica*, 13, pp. 899-901.

Fromm, B.S., Adams, B. L., Ahmadi, S., Knezevic, M. (2009): Grain size and

orientation distributions: Application to yielding of α-titanium, *Acta Materialia*, 57, 8, pp. 2339-2348.

Fullwood, D.T., Kalidindi, S.R., Niezgoda, S.R., Fast, A., Hampson, N. (2008): Gradient-based microstructure reconstructions from distributions using fast Fourier transforms, *Materials Science and Engineering: A*, 494, 1-2, pp. 68-72.

Fullwood, D.T., Niezgoda, S.R., Adams, B.L., Kalidindi, S.R. (2009): Microstructure sensitive design for performance optimization, *Progress in Materials Science*, in press.

Gilormini, P., Toth, L.S., Jonas, J.J. (1990): An analytic method for the prediction of ODFS with application to the shear of FCC polycrystals, *Proc. R. Soc. Lond. A*, 430, pp. 489- 507.

Hicks, N.J. (1965): Notes on differential geometry, *Van Nostrand Reinhold Company*.

Hutchinson, J.W. (1976): Bounds and Self-Consistent Estimates for Creep of Polycrystalline Materials, *Proceedings of the Royal Society of London, Series A, Mathematical and Physical Sciences (1934-1990)*, 348, pp. 101-127.

Irgens, F. (2008): Continuum Mechanics, *Springer-Verlag Berlin Heidelberg*.

Kalidindi, S.R., Anand, L. (1992): An approximate procedure for predicting the evolution of crystallographic texture in bulk deformation processing of fcc metals, *Int. J. Mech. Sci.*, 34, 4, pp. 309-329.

Kalidindi, S.R., Bronkhorst, C. A., Anand L. (1992) Crystallographic Texture Evolution in Bulk Deformation Processing of FCC Metals, *J. Mech. Phys. Solids*, 40, 3, pp. 537-569.

Kalidindi, S.R., Anand, L. (1994): Macroscopic Shape Change and Evolution of Crystallographic Texture in Pre-textured FCC Metals, *J. Mech. Phys. Solids*, 42, 3, pp. 459-490.

Knezevic, M., Kalidindi, S.R., Fullwood, D.T. (2008): Computationally efficient database and spectral interpolation for fully plastic Taylor-type crystal plasticity calculations of face-centered cubic polycrystals, *International Journal of Plasticity*, 24, 7, pp. 1264-76.

Kreiss, H.O., Lorenz, J. (2004): Initial-boundary value problems and the Navier-Stokes equations, *Society for Industrial and Applied Mathematics*.

Kroner, E. (1967): Elastic moduli of perfectly disordered composite materials, *J. Mech. Phys. Solids*, 15, pp. 319-329.

Lai, W.M., Rubin, D., Krempl, E. (1993): Introduction to Continuum Mechanics, *Butterworth-Heinemann Ltd.*, 3rd edition.

Morawiec, A. (2004): Orientations and rotations: computations in crystallographic textures, *Springer-Verlag Berlin Heidelberg*.

Morawiec, A., Field, D.P. (1996): Rodrigues Parameterization for Orientation and Misorientation Distributions, *Philosophical Magazine A*, 73, pp. 1113-1130.

Morawiec, A., Wierzbanowski, K., Jura, J., Baczmanski, A. (1991): Prediction of deformation texture in polycrystals, *Philosophical Magazine A*, 64, 6, pp. 1251-1263.

Savoie, J., Zhou, Y., Jonas, J.J., Macewen, S.R. (1996): Textures induced by tension and deep drawing in aluminum sheets, *Acta Materialia*, 44, 2, pp. 587-605.

Schutz, B.F. (1985): A first course in general relativity, *Cambridge University Press*.

Taylor, G.I. (1938): Plastic strain in metals, *J Inst Metal*, 72, pp. 307-25.

Wierzbanowski, K., Clement, A. (1984): Rotation Field and Continuity Equation for Texture Evolution, *Cryst. Res. Technol.*, 19, pp. 201-212.

Wierzbanowski, K., Ahzi, S., Hihi, A., Berveiller, M. (1986): Rolling Textures Predicted by the Elasto-plastic Self-consistent Model, *Cryst. Res. Tehcnol.*, 21, pp. 395-406.

Zhou Y., Toth L.S., Neale, K.W. (1992): On the stability of the ideal orientations of rolling textures for f.c.c. polycrystals, *Acta Metall. Mater.*, 40, 11, pp. 3179-3193.

Zhou, Y., Jonas, J.J., Neale, K.W. (1996): Behaviour of initial texture components during the plane strain drawing of f.c.c. sheet metals, *Acta Materialia*, 44, 2, pp. 607-619.

Appendix A Continuity equation in the mass space

Based upon the conservation of mass principle, a continuity equation in the real space is presented here. We are interested to formulate the continuity equation in the Eulerian coordinate system, thus a spatial description of the material time derivative of a function, Dϕ / Dt, can be shown as [Lai, Rubin and Krempl (1993)]:

$$
\begin{aligned}
\frac{D\phi}{Dt} &= \left(\frac{\partial \phi}{\partial t}\right)_{X=const} = \left(\frac{\partial \phi}{\partial t}\right)_{x=const} + \left(\frac{\partial x_i}{\partial t}\right)_{X=const} \frac{\partial \phi}{\partial x_i} \\
&= \left(\frac{\partial \phi}{\partial t}\right)_{x=const} + v_i \frac{\partial \phi}{\partial x_i}
\end{aligned}
\tag{17}
$$

where x represents the position of a material particle at time t with regard to a spatial (or Eulerian) coordinate system, and X denotes the position of that material

particle at the beginning of the process ($t = 0$). The velocity of material particle moving in the microstructure is shown as v.

Now if we take an arbitrary volume denoted by Ω, and assume that the bounding closed surface of this region be continuous and denoted by Γ, using the spatial description of the material time derivative, it can be shown that the time derivative of the volume integral over the mass density $\rho(x,t)$ is given by:

$$\frac{D}{Dt} \int_{\Omega} \rho dx = \frac{d}{dt} \int_{\Omega} \rho dx + \oint_{\Gamma} \rho v.\hat{n} ds \tag{18}$$

The principle of conservation of mass for a material region requires that the amount of mass over the entire region does not change with the passage of time; therefore the material derivative of mass density over this region must be zero and we have:

$$\frac{d}{dt} \int_{\Omega} \rho dx = - \oint_{\Gamma} \rho v.\hat{n} ds \tag{19}$$

This equation is known as the control-volume formulation of the conservation of mass principle. Converting the surface integral to a volume integral by means of the divergence theorem, we obtain:

$$\int_{\Omega} \left[\frac{\partial \rho}{\partial t} + div(\rho v) \right] dx = 0 \tag{20}$$

Since this equation must be valid for any arbitrary volume in the mass space, the integral vanishes, and the local form of the conservation of mass principle can be formulated as:

$$\frac{\partial \rho}{\partial t} + div(\rho v) = 0 \tag{21}$$

This equation, called the continuity equation, expresses local conservation of mass at any point in a continuous medium.

Appendix B Forward-backward finite difference scheme

The finite difference method that is used in computation of partial derivatives presented in continuity equations (Eqs. 9 and 12) is explained by a simple example here. Suppose that we have a one-dimensional MF, as in Tab. 3. The MF is taken to be 0 for phase 1 and 1 for phase 2. Furthermore, we suppose that a positive velocity is applied and it deforms the MF such that it moves the MF

one bin to the right. Then, for instance for the mass-based continuity equation, Eq. 9 is simplified to $\Delta M = -v(x)\,(dM(x)/dx)\,\Delta t$. By assuming that $\Delta t = 1$ and that $\Delta x = 1$, for a positive velocity everywhere in the domain we have $v = 1$; Thus the only undetermined term is the partial derivatives for which a forward or backward FDM can be used. As we know the forward FDM adopted for the MF has the form $M_i' = (M_{i+1} - M_i)\,/\Delta x$, and the backward difference has this form: $M_i' = (M_i - M_{i-1})\,/\Delta x$. Therefore, to find the final MF based upon this simplified iteration scheme we will have: $M_f = M_i - vM'\Delta t$. Tab. 3 shows the final MF calculated by the forward and backward differences for a positive velocity. The final MF calculated by the forward difference gives improper values for the MF and it cannot be used for positive velocities; however, the MF predicted by the forward FDM shows that phase 2 is moving to the right under positive velocities.

Table 3: An example of applying forward/backward differences for positive velocities

M_i	0	0	1	1	1	0	0
dM/dx (forward)	0	1	0	0	-1	0	
M_f (forward)	0	-1	1	1	2	0	
dM/dx (backward)		0	1	0	0	-1	0
M_f (backward)		0	0	1	1	1	0

Similarly it can be shown that the forward difference method can be used for negative velocities.

Appendix C Continuity equation in the orientation space

In this section, the continuity equation for orientations is formulated. The continuity equation for orientations is expressed as:

$$\frac{\partial f}{\partial t} + div(fw) = 0 \tag{22}$$

where f is the ODF and w is the velocity vector in the orientation space. The idea here is to find the divergence term in the Euler angle workspace. The EAS is taken as a Riemannian manifold and the divergence is obtained. In a Riemannian manifold, the covariant derivative can be used to find the differentiation of a vector field, with t^i components, on the manifold [Hicks (1965); Schutz (1985)]:

$$t^i_{:j} = \frac{\partial t_i}{\partial x_j} + \Gamma^i_{jk} t^k \tag{23}$$

where Γ^i_{jk} are the Christoffel symbols having a unique canonical connection, called the Levi-Civita connection, with the coordinate systems on the manifold [Morawiec (2004)]:

$$\Gamma^i_{jk} = \frac{1}{2} g^{im} \left(\frac{\partial g_{km}}{\partial x^j} + \frac{\partial g_{im}}{\partial x^k} - \frac{\partial g_{jk}}{\partial x^m} \right) \tag{24}$$

In this equation, g^{ij} is the covariant form of the metric tensor, g_{ij}, and its components are defined by $g^{ij} g_{jk} = \delta^i_k$ where δ^i_k is the Kronecker delta taking 1 if $i = k$, and 0 otherwise.

For Euler angles the components of the metric tensor and its covariant tensor, g^{ij}, are:

$$g_{ij} = \frac{1}{4c} \left(\delta_{ij} + 2\delta_{1(i}\delta_{j)3} \cos\Phi \right)$$

$$g^{ij} = \frac{4c}{\sin^2\Phi} \left(\delta^{ij} - 2\delta^{1(i}\delta^{j)3} \cos\Phi - \delta^{i2}\delta^{j2} \cos^2\Phi \right) \tag{25}$$

where $c = \pi^{4/3}$ and $\delta_{i(j}\delta_{k)l} = \frac{1}{2} \left(\delta_{ij}\delta_{kl} + \delta_{ik}\delta_{jl} \right)$. Similarly $\delta^{i(j}\delta^{k)l} = \frac{1}{2} \left(\delta^{ij}\delta^{kl} + \delta^{ik}\delta^{jl} \right)$. The Christoffel symbols are:

$$\Gamma^i_{jk} = \frac{1}{\sin\Phi} \left(\left(\delta^{i1} \cos\Phi - \delta^{i3} \right) \delta_{1(j}\delta_{k)2} + \left(\delta^{i3} \cos\Phi - \delta^{i1} \right) \delta_{2(k}\delta_{j)3} \right)$$
$$+ \delta^{i2}\delta_{1(j}\delta_{k)3} \sin\Phi \quad (26)$$

Representing the orientation flow field as $J = fw$, one can find the divergence term in Eq. 18 based upon the definition of the covariant derivative: $div(J) = J^i_{;i}$. Using Eq. 23 the divergence can be shown in the form of Christoffel symbols in the EAS:

$$div(J) = J^i_{;i} = \frac{\partial J^i}{\partial g_j} + \Gamma^i_{ij} J^j \tag{27}$$

where $g_i = g(\varphi_1, \Phi, \varphi_2)$ denotes the correspondence Euler angles in the EAS and should not be confused by the metric tensor. It is found that among all Christoffel symbols of the form Γ^i_{ij} only the following terms are not zero: $\Gamma^1_{12} = \Gamma^3_{32} = 1/2\cot\Phi$. Now the final form of the divergence operator will be:

$$div(J) = \frac{\partial J^i}{\partial g_j} + (\Gamma^1_{12} + \Gamma^3_{32})J^2 = \frac{\partial J^i}{\partial g_i} + (\cot\Phi)J^2 \tag{28}$$

We can now place the divergence operator into the continuity equation:

$$\frac{\partial f}{\partial t} = -\frac{\partial J^i}{\partial g_j} - (\cot\Phi)J^2 \tag{29}$$

The final form of the continuity equation in the Euler Angle space can then be obtained by replacing the orientation flow field $J^i = f w_i$:

$$\frac{\partial f}{\partial t} = -f \frac{\partial w_i}{\partial g_i} - w_i \frac{\partial f}{\partial g_i} - f \cot \Phi \, w_2 \tag{30}$$

which represents the conservation of orientation principle in the Eulerian framework.